

DESY/04-087
SFB/PPP-04-14
May 2004

Non-perturbative Pion Matrix Element of a twist-2 operator from the Lattice

M. Guagnelli^a, K. Jansen^b, F. Palombi^{a,c},
R. Petronzio^a, A. Shindler^b and I. Wetzorke^b

Zeuthen-Rome (ZeRo) Collaboration

^a Dipartimento di Fisica, Università di Roma *Tor Vergata*
and INFN, Sezione di Roma II,

Via della Ricerca Scientifica 1, I-00133 Rome, Italy

^b NIC/DESY Zeuthen, Platanenallee 6, D-15738 Zeuthen, Germany

^c *E. Fermi* Research Center, c/o Compendio Viminale, pal. F, I-00184 Rome, Italy

Abstract

We give a continuum limit value of the lowest moment of a twist-2 operator in pion states from non-perturbative lattice calculations. We find that the non-perturbatively obtained renormalization group invariant matrix element is $\langle x \rangle_{\text{RGI}} = 0.179(11)$, which corresponds to $\langle x \rangle^{\overline{\text{MS}}}(2 \text{ GeV}) = 0.246(15)$. In obtaining the renormalization group invariant matrix element, we have controlled important systematic errors that appear in typical lattice simulations, such as non-perturbative renormalization, finite size effects and effects of a non-vanishing lattice spacing. The crucial limitation of our calculation is the use of the quenched approximation. Another question that remains not fully clarified is the chiral extrapolation of the numerical data.

1 Introduction

Deep inelastic scattering [1] continues to provide important information on the structure of hadrons. Phenomenological fits to experimental data give values for the moments of parton distribution functions (PDF), including estimates of their errors, see e.g. [2–4]. Since such moments can be expressed as expectation values of local operators, they are accessible to lattice calculations [5]. A direct comparison of these lattice calculations of moments with the results of the phenomenological fits will test whether these fits are consistent with direct QCD predictions. If we think of, e.g., precise determinations of the strong coupling constant from scaling violations in deep inelastic scattering, such non-trivial checks are mandatory.

Lattice results do not come for free, however: Concepts of non-perturbative renormalization have to be developed; in the process of moving from the continuum of space time to an euclidean lattice a non-vanishing value of a lattice spacing a is introduced, leading to discretization effects; running simulations on a computer necessitates the use of an only finite volume; the limited amount of computing resources leads to the fact that simulations are performed at rather large values of the quark masses that are far from their values assumed in nature. In addition, at present we are left with the quenched approximation, neglecting internal quark degrees of freedom. Finally, the numerical results are plagued by statistical errors that can be substantial for bad choices of operators.

In the course of our work [6–11] to reach a reliable value for a moment of a parton distribution function we eliminated important sources of systematic errors besides the quenched approximation (see [12–14] for summaries of these works). The transition to full dynamical simulations is undertaken world-wide today [15] and the next years will see the exciting results of such calculations. Another open question is the chiral extrapolation that is not understood presently (see [16] and refs. therein).

Let us sketch how we have addressed the systematic errors of the lattice calculations in our work:

- *Non-perturbative renormalization*

We adopt in our work [6, 7, 11] the Schrödinger functional (SF) scheme [17], which has been proved to be a very successful and practical way to compute scale dependent renormalization constants. By evolving deep into the perturbative regime, renormalization group invariant (RGI) quantities can be determined that allow to relate lattice results into any desired continuum renormalization scheme [18–20]. In this paper we compute the renormalization factor at the matching scale (see sect. 3.2 for details).

- *Discretization effects*

We have controlled effects of a non-vanishing lattice spacing a by performing all our lattice calculations with several values of a with two different lattice formulations of lattice QCD: one is the standard Wilson fermion, the other the non-perturbatively improved Wilson fermion formulation. In this way, all

quantities could be extrapolated to their continuum value in a controlled way performing a constrained continuum limit [8, 11]. In particular in this work we have used this strategy to control the continuum limit of the renormalized matrix element.

- *Finite Size Effects*

The finite size effects were controlled in two ways. For the computation of the evolution of the renormalization constants [7, 9, 11], the finite volume Schrödinger functional scheme was used, in which the scale μ is identified with the inverse lattice extent L^{-1} . In this way, the finiteness of the lattice has been utilized to determine the scale dependence.

For the matrix elements, a careful test of finite size effects has been performed [21] with the somewhat surprising result that such effects are rather large for the pion matrix element at a point where the pion mass itself shows no effects. Since this was done for pion matrix elements only, it will be very important to repeat the analysis for baryon matrix elements, where such effects are expected to be even larger [22].

- *Statistical errors*

By employing generalized boundary conditions in space, the signal to noise ratio of operators that need an external momentum could be minimized by optimizing parameters that are introduced by the generalized boundary conditions [11]. This allowed us to obtain results that would not have been possible otherwise.

- *Chiral extrapolation*

The extrapolation of the numerical data from the rather heavy quark masses, where the simulations are performed, to their physical values is still under debate and not clarified, see [16] for a general discussion, and [23–28] for works on the chiral extrapolation of PDF. We will follow the strategy in this work that we first extrapolate the values of our non-perturbatively improved matrix elements to the continuum limit. Comparisons to predictions of chiral perturbation theory are then performed directly in the continuum in order to avoid lattice spacing effects that would render the interpretation difficult.

After having understood and overcome the above difficulties, we can now provide results that are free of these systematic uncertainties besides the, presently still unavoidable, quenched approximation. In this work we summarize our result and, most importantly, we provide the missing part, i.e. the renormalized matrix element at the hadronic scale $\mu_0 \simeq 275$ MeV down to which the scale evolution has been computed ([11]), with a full control on the continuum limit and a careful analysis of the chiral extrapolation. As the most important quantity we consider the *renormalization group invariant* (RGI) matrix element of the twist-2 operator between pion

states corresponding to the first moment of the valence quark distribution, which we find

$$\langle x \rangle_{\text{RGI}} = 0.179(11). \quad (1)$$

This quantity is of central importance since it allows to relate the non-perturbatively obtained results using a particular lattice renormalization scheme to more conventional schemes. For example, if we use the $\overline{\text{MS}}$ scheme, we find that at a scale of 2 GeV the value of the matrix element compares to phenomenological estimates of the same quantities extracted from global fits of experimental data [29] as follows *:

$$\begin{aligned} \langle x \rangle^{\overline{\text{MS}}}(\mu = 2 \text{ GeV}) &= 0.246(15) \\ \langle x \rangle_{phen}(\mu = 2 \text{ GeV}) &= 0.21(2). \end{aligned} \quad (2)$$

This results demonstrates that the running of moments of parton distribution functions in the *continuum* can be calculated from lattice simulations in an intrinsic perturbative scheme like the $\overline{\text{MS}}$ retaining all the non-perturbative information coming from the RGI matrix element. In addition, the errors coming from the lattice simulations are comparable to the experimental errors, which opens the possibility to perform direct tests of QCD as the theory of the strong interaction.

2 Renormalized matrix element

The moments of parton density distributions are related to expectation values of local operators, which are renormalized multiplicatively by applying appropriate renormalization factors $Z(\mu)$ that depend on the energy scale μ (see, e.g. ref. [1]). This leads to consider renormalized matrix elements $O^{\text{ren}}(\mu)$ using some renormalization scheme, denoted by *ren.* For lattice calculations, we are aiming at here, a very useful scheme is the Schrödinger function (SF) renormalization scheme [17] since it applies in small volumes.

If the energy scale μ of $Z(\mu)$ is chosen large enough, it is to be expected, and indeed it can be checked explicitly, that the scale evolution is very well described by perturbation theory, giving rise to the following definition of a *renormalization group invariant* (RGI) matrix element:

$$O_{\text{RGI}} = O^{\text{SF}}(\mu) \cdot f^{\text{SF}}(\bar{g}^2(\mu)) \quad (3)$$

with $\bar{g}(\mu)$ the running coupling computed in the same SF scheme and

$$f^{\text{SF}}(\bar{g}^2) = (\bar{g}^2(\mu))^{-\gamma_0/2b_0} \cdot \exp \left\{ - \int_0^{\bar{g}(\mu)} dg \left[\frac{\gamma(g)}{\beta(g)} - \frac{\gamma_0}{b_0 g} \right] \right\}, \quad (4)$$

*Some details on the extraction of the phenomenological number can be found in sect. 5.1 of this paper.

where $\beta(g)$ and $\gamma(g)$ are the β and anomalous-dimension functions computed to a given order of perturbation theory in a specified scheme, i.e. here the SF scheme. Once we know the value of O_{RGI} evaluated non-perturbatively, the running matrix element in a preferred scheme can be computed, for example in the $\overline{\text{MS}}$ scheme:

$$O^{\overline{\text{MS}}}(\mu) = O_{\text{RGI}}/f^{\overline{\text{MS}}}(g_{\overline{\text{MS}}}^2(\mu)) \quad (5)$$

with now, of course, the β and γ functions computed in the $\overline{\text{MS}}$ scheme. Thus, although the SF is an unphysical finite volume scheme (but therefore most suited for lattice simulations) it can be related to more conventional continuum renormalization schemes by providing the renormalization group invariant quantities.

A non-perturbatively obtained value of the renormalization group invariant matrix element is hence of central importance. Its calculation has to be performed in several steps. The reason is that we have to cover a broad range of energy scales – from the deep perturbative to the non-perturbative region. Using the scale dependent renormalization factor $Z^{\text{SF}}(\mu)$, we write the renormalized matrix element of eq. (3) as

$$O^{\text{SF}}(\mu) = \frac{\langle h|\mathcal{O}|h\rangle}{Z^{\text{SF}}(\mu)}, \quad (6)$$

where $|h\rangle$ is the hadron state we are interested in. So far, all our discussions have been in the continuum. However, if we think of the lattice regularization and eventual numerical simulations to obtain non-perturbative results, it would be convenient to compute the renormalized matrix element at only one (i.e. small hadronic) scale μ_0 . We therefore rewrite the r.h.s. of eq. (6) as

$$\frac{\langle h|\mathcal{O}|h\rangle}{Z^{\text{SF}}(\mu)} = \frac{\langle h|\mathcal{O}|h\rangle}{Z^{\text{SF}}(\mu_0)} \cdot \underbrace{\frac{Z^{\text{SF}}(\mu_0)}{Z^{\text{SF}}(\mu)}}_{\equiv \sigma(\mu/\mu_0, \bar{g}(\mu))}, \quad (7)$$

where we introduce the step scaling function $\sigma(\mu/\mu_0, \bar{g}(\mu))$, which describes the evolution of the renormalization factor from a scale μ_0 to a scale μ . The advantage of concentrating on the step scaling function instead of the renormalization factor itself is that the step scaling function is well defined in the continuum and hence suitable for eventual continuum extrapolations of lattice results. We finally write the r.h.s. of eq. (3) as

$$O_{\text{RGI}} = O^{\text{SF}}(\mu_0) \underbrace{\sigma(\mu/\mu_0, \bar{g}(\mu)) \cdot f^{\text{SF}}(\bar{g}^2(\mu))}_{\equiv \mathfrak{S}_{\text{INV}}^{\text{UV,SF}}(\mu_0)} \quad (8)$$

with $O^{\text{SF}}(\mu_0)$ the renormalized matrix element, which is to be computed only once at a scale μ_0 and the ultraviolet (UV) invariant step scaling function $\mathfrak{S}_{\text{INV}}^{\text{UV,SF}}(\mu_0)$, which still depends on the infrared scale μ_0 , and on the renormalization scheme adopted. In ref. [11] we have given a value for the UV invariant step scaling function and

checked the independence on the ultraviolet scale μ . In this work we will provide the missing part, i.e. the renormalized matrix element at the scale μ_0 . The final result for the renormalized matrix element of the pion that we are going to provide here, was made possible by a number of theoretical and conceptual developments that we could achieve over the last years [6–9]. The methods developed there can immediately be taken over to other matrix elements than the lowest twist case of the pion considered here and to the unquenched situation. Nevertheless, with this paper we want to finish the analysis of the pion matrix element with the aim to have eliminated important systematic uncertainties besides the quenched approximation.

2.1 Transfer matrix decomposition

The moments of parton distribution functions (PDF) are related to matrix elements of leading twist τ ($\tau = \text{dim} - \text{spin}$) operators of given spin, between hadron states $h(p)$

$$\langle h(p) | \mathcal{O}_{\mu_1 \dots \mu_N} | h(p) \rangle = M^{(N-1)}(\mu) p_{\mu_1} \dots p_{\mu_N} + \text{terms } \delta_{\mu_i \mu_j}, \quad (9)$$

$$\langle x^{(N-1)} \rangle(\mu) = M^{(N-1)}(\mu = Q). \quad (10)$$

We concentrate in this work on the twist-2 operator corresponding to the second moment of the parton distribution functions (PDF) between charged pion states. In the following we consider the fermionic fields $\psi(x)$ and $\bar{\psi}(x)$ as doublets in the flavour space. In particular we will concentrate on the valence u or \bar{d} distribution as explained below. This amounts to consider operators of the form

$$\mathcal{O}_{\mu\nu}(x) = \frac{1}{4} \bar{\psi}(x) \gamma_{\{\mu} \overleftrightarrow{D}_{\nu\}} \psi(x) - \delta_{\mu\nu} \cdot \text{trace terms}, \quad (11)$$

where $\{\dots\}$ means symmetrization on the Lorentz indices, $\overleftrightarrow{D}_\mu = \overrightarrow{D}_\mu - \overleftarrow{D}_\mu$ and

$$\overrightarrow{D}_\mu = \frac{1}{2}(\nabla_\mu + \nabla_\mu^*), \quad \overleftarrow{D}_\mu = \frac{1}{2}(\overleftarrow{\nabla}_\mu + \overleftarrow{\nabla}_\mu^*). \quad (12)$$

The definitions of the lattice derivatives and conventions are given in the appendix.

There are two representations of such an operator on the lattice [30]. The first representation takes $\mu \neq \nu$, whereas the second uses $\mu = \nu$. The precise definitions of the operators used here are

$$\mathcal{O}_{12}(x) = \frac{1}{4} \bar{\psi}(x) \gamma_{\{1} \overleftrightarrow{D}_{2\}} \psi(x) \quad (13)$$

and

$$\mathcal{O}_{44}(x) = \frac{1}{2} \bar{\psi}(x) \left[\gamma_4 \overleftrightarrow{D}_4 - \frac{1}{3} \sum_{k=1}^3 \gamma_k \overleftrightarrow{D}_k \right] \psi(x). \quad (14)$$

In computing the matrix elements of these operators, a non-zero momentum in two different spatial directions has to be supplied for $\mathcal{O}_{12}(x)$ in eq. (13), whereas for the operator $\mathcal{O}_{44}(x)$ in eq. (14) no momentum is needed. It is to be expected, and indeed verified in numerical simulations, that the signal of the matrix element of $\mathcal{O}_{44}(x)$ is better than the one of $\mathcal{O}_{12}(x)$. Thus in the following investigation we consider only $\mathcal{O}_{44}(x)$.

Our setup of lattice QCD is on a hyper-cubic euclidean lattice with spacing a and size $L^3 \times T$. We impose periodic boundary conditions in the spatial directions and Dirichlet boundary conditions in time, as they are used to formulate the Schrödinger functional (SF) [17] (we refer to these references for unexplained notations). Using homogeneous boundary conditions, where the spatial components of the gauge potentials at the boundaries and also the fermion boundary fields are set to zero, the Schrödinger functional partition function can be written as [31]

$$\mathcal{Z} = \langle i_0 | e^{-T\mathbb{H}} \mathbb{P} | i_0 \rangle, \quad (15)$$

where the initial and final states $|i_0\rangle$ carry the quantum numbers of the vacuum and \mathbb{P} denotes a projector on gauge invariant states. The states with charged pion quantum numbers in the Schrödinger functional are, indicating with ζ and $\bar{\zeta}$ (and the corresponding ζ' and $\bar{\zeta}'$) a flavour doublet, the dimensionless fields

$$\mathbb{S} = \frac{a^6}{L^3} \sum_{\mathbf{y}, \mathbf{z}} \bar{\zeta}(\mathbf{y}) \gamma_5 \tau^+ \zeta(\mathbf{z}) \quad \text{and} \quad \mathbb{S}' = \frac{a^6}{L^3} \sum_{\mathbf{u}, \mathbf{v}} \bar{\zeta}'(\mathbf{u}) \gamma_5 \tau^- \zeta'(\mathbf{v}), \quad (16)$$

where $\tau^\pm = \frac{1}{\sqrt{2}}(\tau^1 \pm i\tau^2)$ and τ^k with $k = 1, 2, 3$ are the usual Pauli matrices. The pion interpolating fields \mathbb{S} and \mathbb{S}' are respectively localized at $x_0 = 0$ and $x_0 = T$. The desired matrix element is obtained from the correlation function

$$f_{44}(x_0) = -\frac{1}{2} \langle \mathbb{S}' \mathcal{O}_{44}(x) \mathbb{S} \rangle, \quad (17)$$

where we have used the independence on the spatial components \mathbf{x} of $x = (x_0, \mathbf{x})$. The Wick contractions of this correlation function contain also a disconnected piece that we neglect consistently with the fact that we are interested on valence quark distribution. For normalization purposes it is important to define the boundary to boundary correlation function

$$f_1 = -\frac{1}{2} \langle \mathbb{S}' \mathbb{S} \rangle. \quad (18)$$

The basic fermionic Wick contractions for these two correlation functions are depicted in fig. 1.

In the following we will denote with $|i_0\rangle$ and $|i_\pi\rangle$ the states carrying respectively the quantum numbers of the vacuum and of the charged pion at zero momentum. The correlation functions f_{44} and f_1 have the following quantum mechanical representations

$$f_{44}(x_0) = \mathcal{Z}^{-1} \frac{1}{2} \langle i_\pi | e^{-(T-x_0)\mathbb{H}} \mathbb{P} \mathcal{O}_{44} e^{-x_0\mathbb{H}} \mathbb{P} | i_\pi \rangle, \quad (19)$$

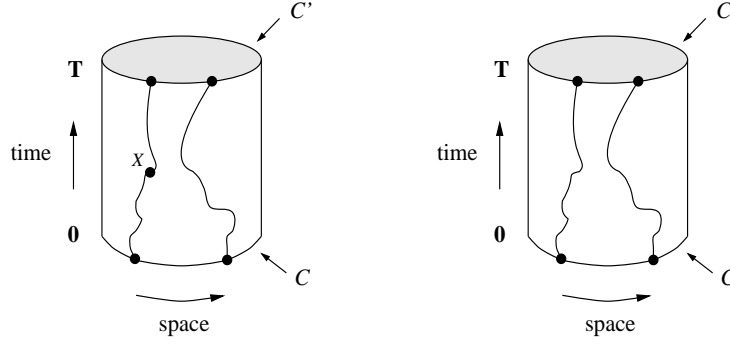


Figure 1: Fermionic Wick contractions for the f_{44} and f_1 correlators. C and C' denote the boundary gauge field respectively at $x_0 = 0$ and $x_0 = T$; x denotes the insertion point of the local operator.

$$f_1 = \mathcal{Z}^{-1} \frac{1}{2} \langle i_\pi | e^{-T\mathbb{H}} \mathbb{P} | i_\pi \rangle . \quad (20)$$

In order to extract the pion mass we have analyzed also the improved axial correlation function

$$f_A^I(x_0) = -\frac{L^3}{2} \langle A_0^I(x) \mathbb{S} \rangle , \quad (21)$$

where

$$A_0^I(x) = A_0(x) + ac_A \frac{1}{2} (\partial_0^* + \partial_0) P(x) ; \quad (22)$$

c_A is the improvement coefficient and the axial and pseudoscalar local operators take the form

$$A_0(x) = \bar{\psi}(x) \gamma_0 \gamma_5 \tau^- \psi(x) \quad (23)$$

$$P(x) = \bar{\psi}(x) \gamma_5 \tau^- \psi(x). \quad (24)$$

The non-perturbative value of c_A was taken from ref. [32].

Following ref. [31] we insert a complete set of eigenstates of the hamiltonian and, retaining only the first non-leading corrections, we have for the improved axial current correlation function $f_A^I(x_0)$ and f_1 ,

$$f_A^I(x_0) \simeq \frac{L^3}{2} \rho \langle 0, 0 | A_0^I | 0, \pi \rangle e^{-m_\pi x_0} \{ 1 + \eta_A^\pi e^{-x_0 \Delta} + \eta_A^0 e^{-(T-x_0)m_G} \} \quad (25)$$

$$f_1 \simeq \frac{1}{2} \rho^2 e^{-m_\pi T} . \quad (26)$$

where the coefficient appearing in this expansions are

$$\rho = \frac{\langle 0, \pi | i_\pi \rangle}{\langle 0, 0 | i_0 \rangle}, \quad (27)$$

$$\eta_A^\pi = \frac{\langle 0, 0 | A_0^I | 1, \pi \rangle \langle 1, \pi | i_\pi \rangle}{\langle 0, 0 | A_0^I | 0, \pi \rangle \langle 0, \pi | i_\pi \rangle}, \quad (28)$$

$$\eta_A^0 = \frac{\langle i_0 | 1, 0 \rangle \langle 1, 0 | A_0 | 0, \pi \rangle}{\langle i_0 | 0, 0 \rangle \langle 0, 0 | A_0 | 0, \pi \rangle}. \quad (29)$$

The energy gap in the pion channel between the fundamental and the first excited state is denoted by Δ and is estimated to be $\Delta r_0 \approx 3.2$, while m_G is the mass of the 0^{++} glueball, $m_G r_0 \approx 4.3$ [31]. For the matrix element we find

$$f_{44}(x_0) \simeq \frac{1}{2} \rho^2 \langle 0, \pi | \mathcal{O}_{44} | 0, \pi \rangle e^{-m_\pi T} \{ 1 + \eta_{\mathcal{O}_{44}}^\pi e^{-x_0 \Delta} + \eta_{\mathcal{O}_{44}}^\pi e^{-(T-x_0)\Delta} \}, \quad (30)$$

where we define the ratio

$$\eta_{\mathcal{O}_{44}}^\pi = \frac{\langle 0, \pi | \mathcal{O}_{44} | 1, \pi \rangle \langle 1, \pi | i_\pi \rangle}{\langle 0, \pi | \mathcal{O}_{44} | 0, \pi \rangle \langle 0, \pi | i_\pi \rangle}. \quad (31)$$

A corresponding transfer matrix decomposition is obtained for the correlation function f_{12} . From these expressions it becomes clear that the matrix element we are interested in, neglecting contributions from excited states, can then be extracted from the plateau value of the following ratio:

$$\frac{f_{44}(x_0)}{f_1} = \langle 0, \pi | \mathcal{O}_{44} | 0, \pi \rangle. \quad (32)$$

Finally, in order to relate this numerically computed ratio with the corresponding continuum operators in Minkowski space, we need a suitable normalization factor

$$\langle x \rangle = \frac{2\kappa}{m_\pi} \langle 0, \pi | \mathcal{O}_{44} | 0, \pi \rangle \quad (33)$$

with κ the standard hopping parameter of the Wilson-Dirac-operator. We remark here that $\langle x \rangle$ corresponds to the valence distribution of a single quark (u or \bar{d} for example). We followed ref. [31] in order to extract the plateau values for the effective pion mass and the matrix elements. Using the transfer matrix decomposition in eq.(25), the effects of higher excited states for the effective mass are given by

$$m_{eff}(x_0) \simeq m_\pi + \Delta \eta_A^\pi e^{-\Delta x_0} - m_G \eta_A^0 e^{-m_G (T-x_0)}. \quad (34)$$

In fig. 2 we show the effective pion mass as function of the anticipated excited state contaminations given in eq. (34). From the linear behaviour of the effective mass as a function of $e^{-\Delta x_0}$ and $e^{-m_G (T-x_0)}$ we conclude that these are indeed the leading corrections.

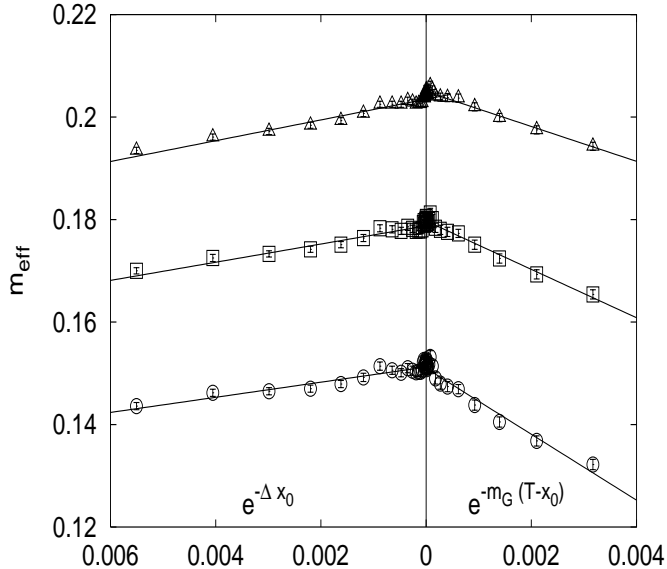


Figure 2: Effective pion mass as a function of the theoretically expected excited state contributions obtained from a transfer matrix decomposition. Data corresponds to the simulation point at $\beta = 6.45$ for three κ values with the non-perturbatively improved action (see table 2). In the left panel we plot the effect of an excited pion state, whereas in the right panel we show the effects of the glueball contribution.

The contribution from excited states on the plateau value of the matrix element following eqs. (26) and (30) is given by

$$\langle x \rangle(x_0) \simeq \langle x \rangle \left\{ 1 + \eta_{\mathcal{O}_{44}}^\pi (e^{-\Delta x_0} + e^{-\Delta (T-x_0)}) \right\} . \quad (35)$$

We show in fig. 3 the matrix element as a function of the expected excitation in eq. (35). Again we observe a linear behaviour of the matrix element indicating that the corrections come mainly from the first excited pion state. It is important to remark that m_G and Δ have been computed using different boundary conditions (see ref. [31]), where in principle excited states corrections have different amplitudes. The agreement between the data and the expected form is then reassuring that the excited states contamination is well controlled.

From fig. 2 and fig. 3 we can read off, what is the systematic error on the pion mass or the matrix element value if a particular value of the time separation x_0 is taken to extract their values. In our analysis, we demanded a systematic relative error, for all the β and k values, coming from the excited states of 0.1% for the pion mass and 0.4% for the matrix element which is well below the statistical accuracy of our computations. Relating the value of x_0 to physical units, the above choice for our desired accuracy leads to a window for the extraction of the plateau that for all the β and k values are around

$$- 1.2 \text{ fm} \lesssim x_0 \lesssim T-1.1 \text{ fm for } m_{\text{eff}},$$

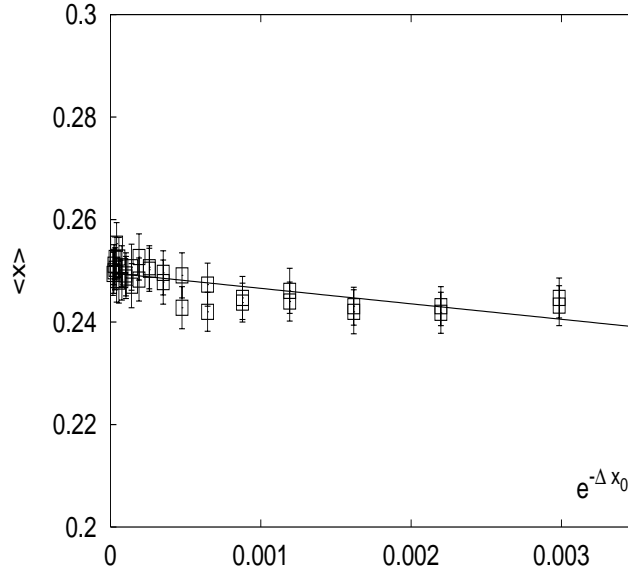


Figure 3: Matrix element as a function of the excited state contribution as obtained from a transfer matrix decomposition. Data corresponds to the simulation point at $\beta = 6.45$ for $\kappa = 0.1350$ with the non-perturbative improved action (see table 2). In the plot we superimpose the results for $x_0 > T/2$ and $x_0 < T/2$.

- $1.3 \text{ fm} \lesssim x_0 \lesssim T-1.3 \text{ fm}$ for the matrix element.

We give in fig. 4 an example for the plateau behaviour of the effective mass and in fig. 5 an example for the plateau behaviour of the matrix element. In table 2 we summarize the time intervals chosen for m_π and $\langle x \rangle$ that fulfill the aforementioned conditions.

3 Numerical details and results

In this section we will give numerical details and results about the computation of the bare matrix element and of the renormalization constant at the low energy scale μ_0 .

3.1 Bare matrix element

We have performed a set of quenched simulations for five β values, varying the lattice spacing between $a = 0.093 \text{ fm}$ and $a = 0.048 \text{ fm}$, see table 1.

In order to have a better control over the continuum extrapolation of our lattice results we performed two independent sets of simulation at these β values, one employing standard Wilson fermions and the other using non-perturbatively $O(a)$ -improved Wilson fermions [32, 33]. As mentioned already above, we used the

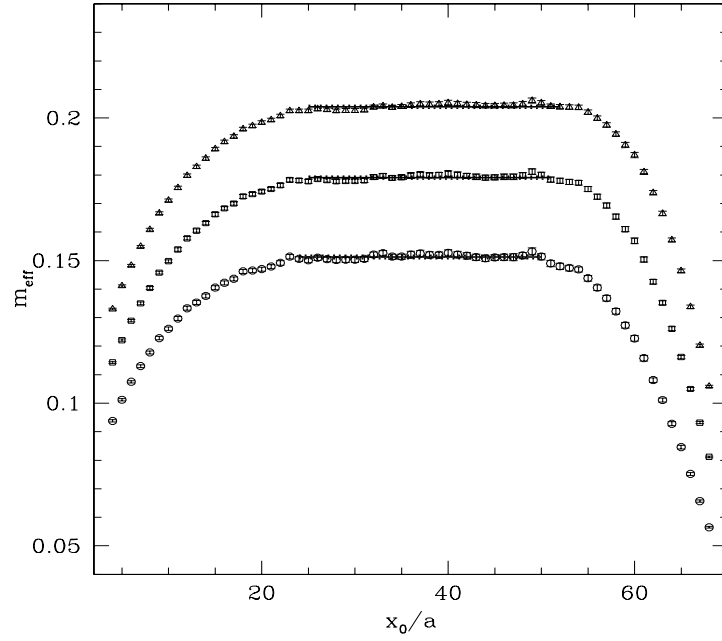


Figure 4: Plateaux for the effective pion mass. The fit region to extract the mass is indicated as a solid line. The simulation was done at $\beta = 6.45$.

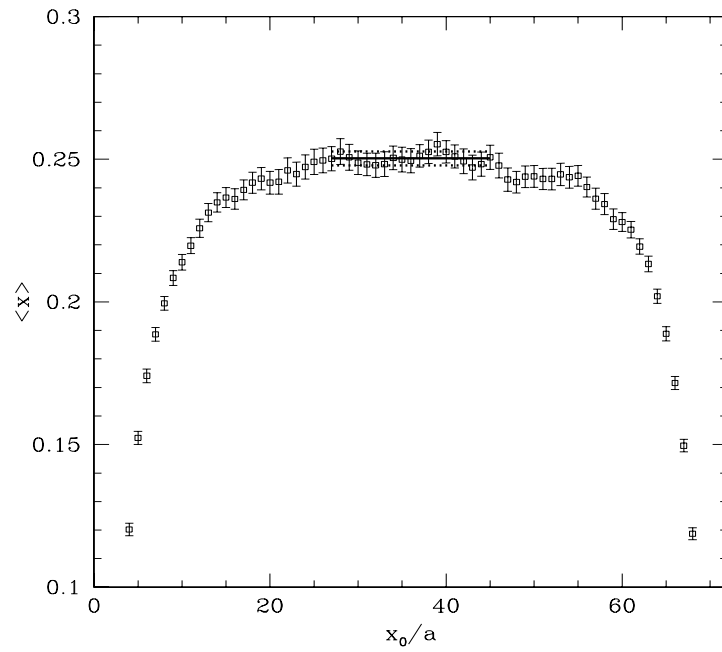


Figure 5: Plateau for the matrix element. The fit region to extract the mass is indicated as a solid line. The simulation was done at $\beta = 6.45$.

$\beta = 6/g_0^2$	r_0/a	L/a	T/a	N
6.0	5.37(2)	16	32	600
6.1	6.32(3)	24	42	600 (Wilson)
6.1	6.32(3)	32	56	185 (Clover)
6.2	7.36(3)	24	48	600
6.3	8.49(4)	24	64	400
6.45	10.46(5)	32	72	400

Table 1: Parameters of our simulation points. N denotes the number of measurements taken into account. For all β -values except for $\beta = 6.1$ the number of measurements refers to Wilson and Clover simulations individually.

quenched approximation throughout this work. In order to achieve an extrapolation to the chiral limit, we employed three values of the quark mass corresponding to a value of m_π that lies in the range of 550 MeV - 1 GeV for all the β values. For the simulations of the lightest quark mass at each β value (the corresponding pion masses range in $4.5 \leq m_\pi L \leq 5.2$), we have corrected for the finite size effects, following ref. [21]. For all the β values the finite size corrections are in the region 0.5%–1.3%. The summary of our bare results in table 2 are thus free from finite size effects. The systematics coming from the higher excited states have been controlled as explained in the previous section.

3.2 Renormalization constant

In order to renormalize the bare matrix element at the scale μ_0 , where we can make contact to the running described by the non-perturbatively computed UV invariant step scaling function $\mathfrak{S}_{\text{INV}}^{\text{UV,SF}}(\mu_0)$, we have to compute the renormalization constants $Z^{\text{SF}}(\mu_0)$. The continuum limit of the renormalized matrix element requires to compute $Z^{\text{SF}}(\mu_0)$ at exactly the lattice spacing, where the matrix element has been calculated, while keeping the scale fixed. Decreasing the lattice spacing a , we would hence have to increase the lattice volume in order to stay at a fixed value of $\mu_0 = (1.436r_0)^{-1}$. Since we can not vary the lattice size continuously, we performed instead simulations on a sequence of lattice sizes and adjusted the values of β to realize the correct value of μ_0 . The values of β are slightly different from the ones used in ref. [34], and were obtained [35] using a new determination of r_0/a [36]. We recall that for our determination of the renormalization constant at the scale μ_0 using the finite volume SF scheme we have performed simulations directly at $\kappa = \kappa_c$, determined through the PCAC Ward identity. Details about the computation of the renormalization factor, such as renormalization condition and external parameters typical of the SF scheme, can be found in ref. [11]. We give in table 3 the parameters of our runs and the values of the Z factors at μ_0 for both Wilson and O(a)-improved Wilson fermions.

In order to match the β values where the matrix elements themselves have been

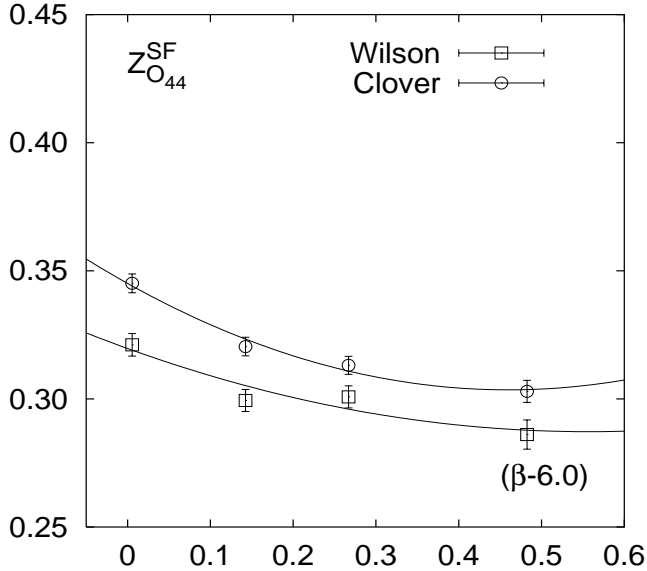


Figure 6: Numerical results for $Z_{\mathcal{O}_{44}}^{\text{SF}}(g_0, \mu_0)$ together with their interpolating polynomials.

computed, we describe the β dependence by an effective interpolation formula,

$$Z^{\text{SF}}(\mu_0) = \sum_{i=0}^2 z_i^{\text{SF}} (\beta - 6.0)^i \quad (36)$$

with the coefficients for Wilson and O(a)-improved Wilson fermions listed in table 4. The statistical uncertainty to be taken into account when using this formula is about 1.1% for the non-perturbatively improved clover action and 1.4% for the Wilson action[†]. In fig. 6 we show the β dependence of $Z^{\text{SF}}(\mu_0)$ for the \mathcal{O}_{44} operator and for the two actions used, together with the plot of the interpolating formula (36).

Using this interpolation formula, we can match the values of a corresponding to the β values used for the computation of the bare matrix element, which allows finally to obtain the renormalized matrix element at the scale μ_0 in the continuum limit.

We have performed a continuum extrapolation at fixed values of $(r_0 m_\pi)^2$. Fixing $(r_0 m_\pi)^2$ is achieved by interpolating our bare matrix elements linearly in the quark mass. The physical values of the pion mass range $550 \text{ MeV} < m_\pi < 1 \text{ GeV}$. In fig. 7 we show an example of the continuum limit at our next to lowest pion mass

[†]For $\beta \approx 6.5$ the error to be associated grows to 1.4% for the non-perturbatively improved clover action and to 2.0% for the Wilson action.

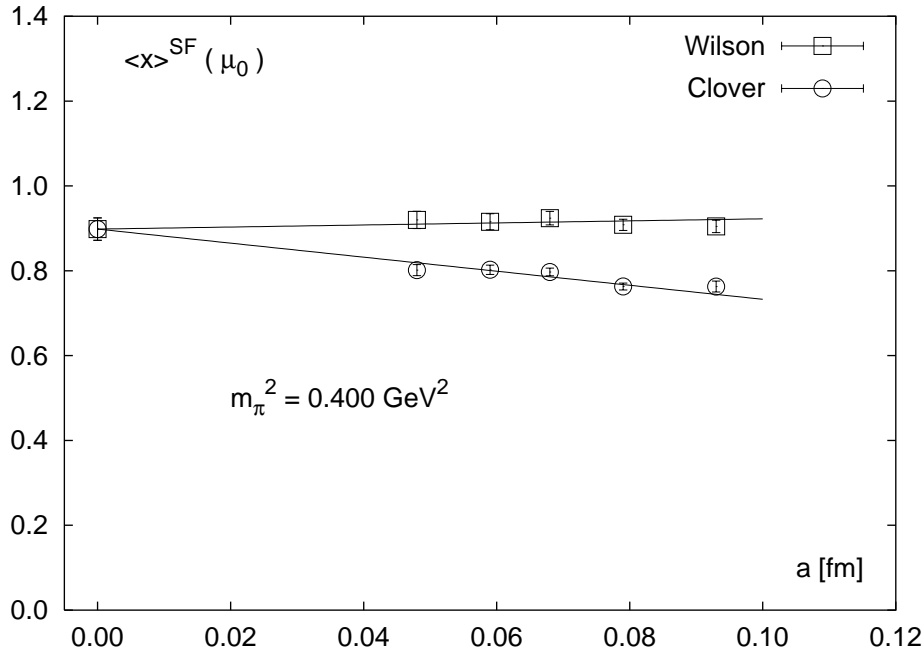


Figure 7: Combined continuum extrapolation for the pion matrix element computed with Wilson and O(a)-improved Wilson fermions, at $(r_0 m_\pi)^2 = 2.57$, which corresponds to a pion mass of $m_\pi = 632$ MeV.

$((r_0 m_\pi)^2 = 2.57)$. The continuum extrapolation of the renormalized matrix element

$$\langle x \rangle^{SF}(\mu_0, r_0 m_\pi) = \lim_{a \rightarrow 0} \frac{\langle \pi | \mathcal{O}_{44} | \pi \rangle(a, r_0 m_\pi)}{Z^{SF}(a, \mu_0)}, \quad (37)$$

has been done via a constrained linear fit in the lattice spacing a using simulation results obtained with the Wilson and clover action. For all the values of the pion mass we have performed this constrained extrapolation excluding the coarsest lattice of our data set. In section 5 we will discuss the uncertainties connected with the continuum extrapolation, and the one related to the chiral extrapolation. If we perform the chiral extrapolation linearly in the pion mass squared directly in the continuum we obtain a value of

$$\langle x \rangle^{SF}(\mu_0) = 0.810(33) \quad (38)$$

for the continuum renormalized pion matrix element in the SF scheme.

We can anticipate here for clarity that, in this particular case, to invert the order of the chiral and continuum extrapolation gives a fully consistent result, independently on how the continuum extrapolation is performed.

4 RGI matrix element

The phenomenological analysis of the experimental data is usually done in the $\overline{\text{MS}}$ scheme. In order to translate our fully non-perturbatively computed matrix element $\langle x \rangle^{SF}(\mu_0)$ renormalized in the SF scheme to the $\overline{\text{MS}}$ scheme, we need first to calculate the universal renormalization group invariant matrix element. This is done following the complete non-perturbative evolution [11] of the step scaling function in the SF scheme as outlined above. Using the UV invariant step scaling function as determined in our earlier work [11], it is now possible to eliminate any reference to the scale μ_0 and to obtain finally the RGI matrix element. In ref. [11] we have already computed

$$\mathfrak{S}_{INV}^{UV,SF}(\mu_0) = 0.221(9). \quad (39)$$

Thus using formula (8) we can obtain the main result of this paper

$$\langle x \rangle_{RGI} = \langle x \rangle^{SF}(\mu_0) \mathfrak{S}_{INV}^{UV,SF}(\mu_0) = 0.179(11). \quad (40)$$

The RGI matrix element allows a simple conversion to any desired scheme (e.g. $\overline{\text{MS}}$ at 2 GeV) requiring only the knowledge of the β - and γ -function up to a certain order in perturbation theory in this scheme [37, 38]. The total renormalization factor to directly translate any bare matrix element of \mathcal{O}_{44} into the RGI matrix element, can be written as

$$Z_{RGI}(g_0) = \frac{Z^{SF}(g_0, \mu_0)}{\mathfrak{S}_{INV}^{UV,SF}(\mu_0)}. \quad (41)$$

Combining eq. (39) and the interpolating formula (36) we obtain a further interpolating polynomial

$$Z_{RGI} = \sum_{i=0}^2 z_i^{\text{RGI}} (\beta - 6.0)^i \quad (42)$$

whose coefficients are listed in table 4. These parametrizations of Z_{RGI} are to be used with the same uncertainty of Z^{SF} and an additional error of 4.0%, coming from the uncertainty of $\mathfrak{S}_{INV}^{UV,SF}(\mu_0)$, that has to be added quadratically after performing a continuum extrapolation. Our resulting number $\langle x \rangle^{\overline{\text{MS}}}(\mu=2\text{GeV})=0.246(15)$ is not fully compatible with previous lattice computation [40], where it was found that $\langle x \rangle^{\overline{\text{MS}}}(\mu=2.4\text{GeV})=0.273(12)$, and in better agreement with the result coming from the global fits [29] of experimental data $\langle x \rangle_{phen}(\mu = 2\text{GeV}) = 0.21(2)$. The disagreement of these numbers could be explained by the fact that in this paper we analyze and correct for several sources of systematic errors. We apply a non-perturbative renormalization and perform the continuum limit, while in [40] a perturbative renormalization was adopted without performing the continuum limit (only one lattice spacing). Moreover we correct, where present, for finite size effects.

5 Chiral and continuum extrapolation

Since the form of the correct chiral extrapolation of the lattice data obtained at rather large quark masses is still under debate (see [16] for a recent review and refs. therein, while for the problem considered here see [23–28]), we aimed at avoiding a possible source of systematic error and *first* performed a continuum extrapolation and *then* tried to extrapolate the data to the chiral limit. In this way, continuum chiral perturbation theory is applicable and we do not have to worry that chiral symmetry breaking effects may spoil the chiral extrapolation at non-vanishing values of the lattice spacing. We fixed the physical values of the pion mass in units of r_0 [39] and performed a continuum extrapolation keeping $r_0 m_\pi$ fixed. To this end we had to slightly interpolate the values of the matrix elements, since in our simulations the pion mass at different values of β were not obtained at the same value of the physical pion mass. The corresponding error, taking the correlations into account, of this slight interpolation is, however, well below the statistical accuracy of our numerical data. We have performed the continuum limit of the matrix element from our simulation points using three, four and five values of β , employing Wilson and O(a)-improved Wilson fermions, in order to study the effect of including coarser lattices for the continuum extrapolation. This detailed analysis is summarized in fig. 8. In all the following discussion, when we talk about chiral extrapolation, we use a linear extrapolation in the squared pion mass.

In this figure we plot the value of $\langle x \rangle^{\overline{\text{MS}}}(\mu = 2 \text{ GeV})$ as a function of the number of points used to perform the continuum extrapolation. Moreover, for each choice of the number of points used, we compare several ways to perform the continuum and chiral limit (the symbols refer to the symbols in fig. 8):

- 1) first the constrained continuum limit and then the chiral extrapolation (∇);
- 2) first the chiral extrapolation and then the constrained continuum limit (\triangle);
- 3) first the chiral extrapolation, then the cont. limit using only the Wilson data (\square);
- 4) first the chiral extrapolation, then the cont. limit using only the clover data (\circ).

All these lattice results are compared with the same quantity obtained through global fits of the experimental data [29]. Our conclusions, for this quantity and for the range of masses and lattice spacings simulated are twofold. First of all, the order of how to perform the chiral and continuum extrapolation is irrelevant, independently from which action is used to do the continuum limit. Then the continuum limit is consistent if performed using three, four or five points, also in this case, independently of the lattice action used.

We decided to perform first the continuum limit at fixed pion mass using the four points corresponding to the four smallest lattice spacings. Only as a second step we then perform the chiral extrapolation linearly in the squared pion mass. The continuum extrapolated data at fixed m_π^2 are collected in table 5.

A remark is in order here. It has been shown in ref. [25] that in quenched chiral perturbation theory (Q χ PT) at the leading order, this particular matrix element is free from chiral logarithms. In ref. [27] it has been shown that in the full χ PT

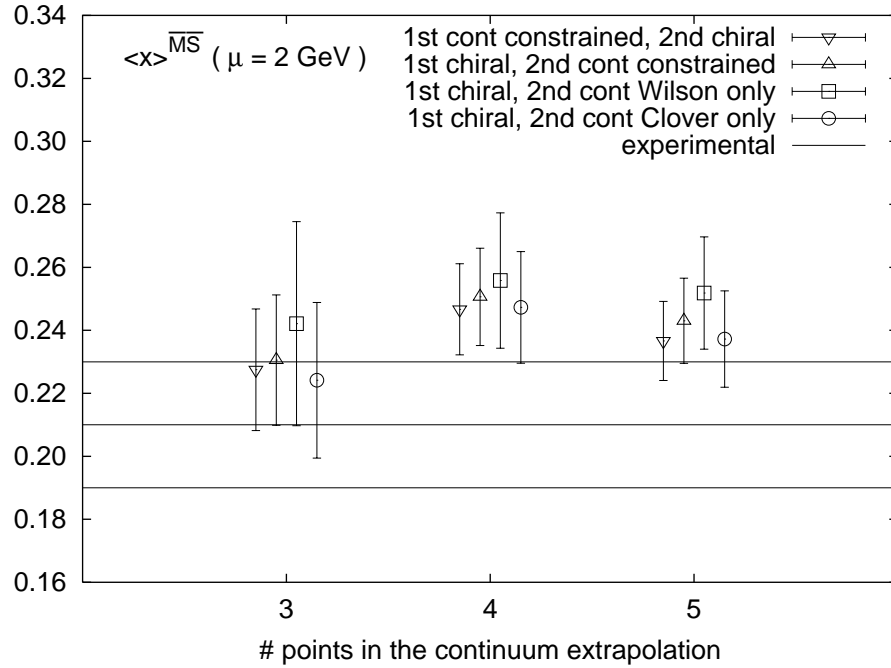


Figure 8: Value of $\langle x \rangle^{\overline{MS}}(\mu = 2 \text{ GeV})$, obtained from our lattice simulations, as a function of the number of points used to perform the continuum extrapolation. For each choice of the number of points used we compare several ways to perform the continuum and chiral limit: (∇) first the constrained continuum limit and then the chiral extrapolation; (\triangle) first the chiral extrapolation and then the constrained continuum limit; (\square) first the chiral extrapolation and then the continuum limit using only the Wilson data; (\circ) first the chiral extrapolation and then the continuum limit using only the clover data. The band represents the same quantity, with its error, obtained through global fits of the experimental data [29].

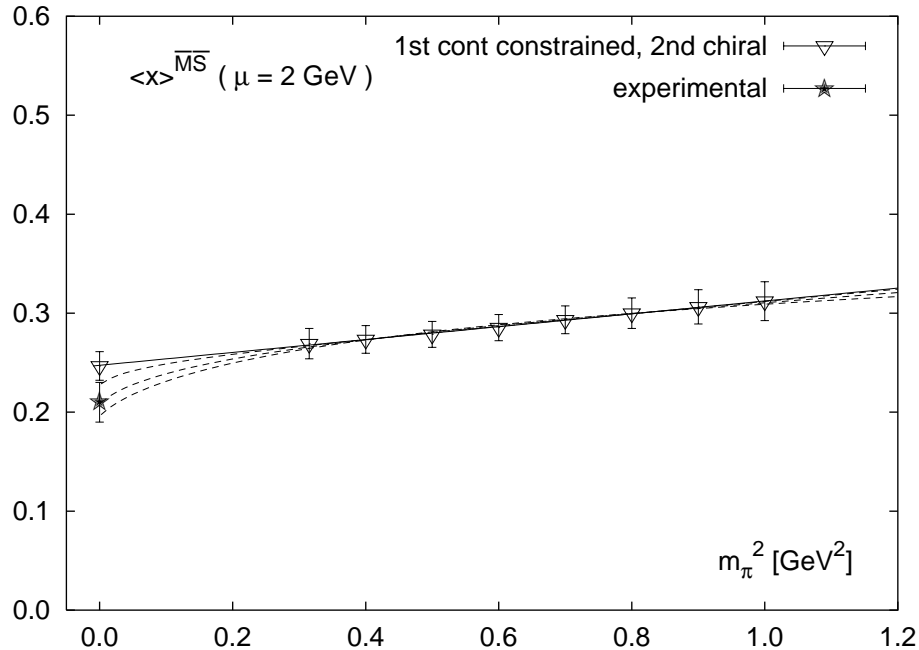


Figure 9: Chiral extrapolation *in the continuum*. The dashed curves refer to the formula (43) with $\Lambda = \{0.4, 0.7, 1.0\}$ GeV and $f_\pi = 93$ MeV. The chiral extrapolated value (∇) is compared with the phenomenological estimate (\star).

indeed there are chiral logarithms. In ref. [24] an effective phenomenological ansatz is given by

$$\langle x^n \rangle = A_n \left[1 - \frac{1}{(4\pi f_\pi)^2} m_\pi^2 \ln \left(\frac{m_\pi^2}{m_\pi^2 + \Lambda^2} \right) \right] + B_n m_\pi^2, \quad (43)$$

motivated by the chiral expansion in the full theory. A similar formula was suggested to explain the discrepancy between the lattice results and the global fits of the experimental data of the proton $\langle x \rangle$.

In fig. 9 we show the *continuum* values of the renormalized matrix elements as a function of the pion mass (see table 5). In order to illustrate possible unquenching effects we also perform a chiral extrapolation using eq.(43). For the different dashed curves in fig. 9 we used different values of the parameter $\Lambda = \{0.4, 0.7, 1.0\}$ GeV that is supposed to provide an estimate of the size of the pion cloud. However, the data, even in the continuum limit, clearly prefer a straight line extrapolation consistent with the results of $\text{Q}\chi\text{PT}$. Using a linear chiral extrapolation we obtain a final value for our matrix element consistent with the experimental results, up to quenching effects. In order to disentangle the quenched and chiral uncertainties, lattice data have to be provided very close to the physical point, where the pion assumes a mass as measured in experiment; presumably chiral invariant formulations of QCD are necessary to clarify the question of the chiral extrapolation. For the time being and

for this work we take the straight line behaviour as suggested by the numerically obtained data for the chiral extrapolation.

5.1 Discussion and concluding remarks

The main results of our paper, i.e. the renormalization group invariant matrix element and the renormalized matrix element at a scale of 2 GeV in the $\overline{\text{MS}}$ scheme, are summarized in eqs. (1,2). Comparing our results to phenomenological estimates, it comes out to be slightly higher, but already more precise than the latest NLO analyses of Drell-Yan and prompt photon πN data [29], which yield a combined experimental value of $\langle x \rangle^{\overline{\text{MS}}}(\mu=2\text{GeV}) = 0.21(2)$. These results have been computed for the valence quark distribution [‡]. We conclude that the non-perturbatively obtained number for the twist-2 matrix element of a pion is not completely consistent with phenomenological estimates. Although this should not be too worrisome, since we are still left with the quenched approximation, it is worthwhile to discuss the lattice numbers further.

One cause for the deviation could lie in the chiral extrapolation of this matrix element that was done linearly in the pion mass. If we would use the phenomenological fit ansatz of ref. [24], we find $\langle x \rangle^{\overline{\text{MS}}}(2\text{GeV}) = 0.21(1)(2)$, where the first error corresponds to varying the data in their errorbars and the second error is the variation for Λ in the range 0.4 to 1.0 GeV. Clearly this chiral extrapolation would reconcile the lattice results with experiments. However, as can be seen in fig. 9, at the moment it is not possible to test such an ansatz unambiguously, since the values of quark masses used in the simulations are too large. Only with future simulations, presumably employing e.g. chiral invariant formulations of lattice QCD, this question could be clarified.

Another cause of the deviation could certainly be the quenched approximation, which is a severe limitation and effects of dynamical quarks have to be explored in the future. In any case, we conclude that the Schrödinger functional method has been proven to provide an excellent tool to compute the non-perturbative scale evolution of multiplicatively renormalized quantities such as the quark mass [34] or the matrix elements [11] considered in this work.

In order to further utilize our results, we attempted to use the non-perturbatively obtained renormalization constants to see the effect of a non-perturbative renormalization on the results of other groups on the quenched bare matrix element of the \mathcal{O}_{44} operator between proton states (preliminary results can be found in [41]).

The LHPC coll. [43] has computed the bare matrix element of the \mathcal{O}_{44} operator between proton states at $\beta = 6.0$ using the Wilson action. The QCDSF coll. [42] has computed the bare matrix element of the \mathcal{O}_{44} operator between proton states at $\beta = 6.0, 6.2, 6.4$ using the non-perturbatively improved clover action. Both the collaborations perform a chiral extrapolation linear in the quark mass at fixed lattice

[‡]We remark here that, as stated in ref. [29], the extraction of the sea distribution in a pion is currently impossible due to the lack of the necessary data at low Bjorken x .

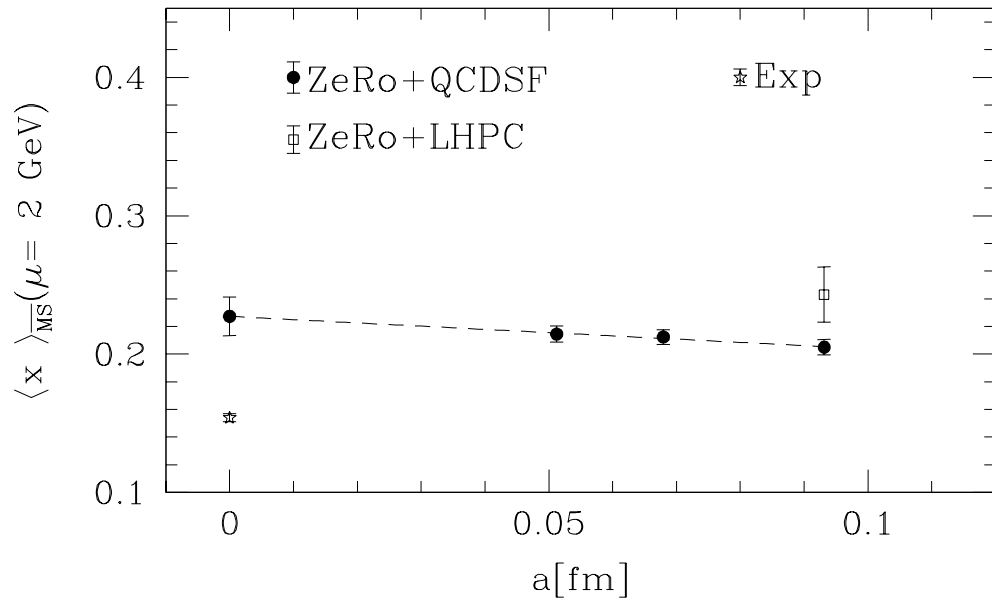


Figure 10: Continuum extrapolation of the non-perturbatively renormalized matrix element of \mathcal{O}_{44} between proton states based on the quenched bare data, both already chirally extrapolated linearly in the quark mass, from refs. [42] and [43], using the non-perturbatively computed Z factor of the present work (ZeRo coll.)

spacing. If we take now the non-perturbative renormalization factor computed in this paper (ZeRo coll.), we obtain the result summarized in fig. 10, where we show the continuum extrapolation of the non-perturbatively renormalized matrix element of \mathcal{O}_{44} between proton states based on the bare data, already chirally extrapolated, from refs. [42], and as a comparison the same non-perturbatively renormalized matrix element using the bare data of ref. [43]. In fig. 10 we also indicate the result obtained from global fits of the experimental data as listed in ref. [43] (see refs. inside for details). The final numerical results are

$$\langle x \rangle^{\overline{\text{MS}}}(\mu = 2\text{GeV}) = 0.227(14) \quad \text{ZeRo} + \text{QCDSF} \quad (44)$$

$$\langle x \rangle^{\overline{\text{MS}}}(\mu = 2\text{GeV}) = 0.243(20) \quad \text{ZeRo} + \text{LHPC} \quad \beta = 6.0 \quad (45)$$

$$\langle x \rangle^{\overline{\text{MS}}}(\mu = 2\text{GeV}) = 0.154(3) \quad \text{global fits} \quad (46)$$

For the first time a continuum extrapolation in the case of the proton matrix element could be done, thanks to the non-perturbative renormalization factor computed in this paper.

Acknowledgments

We thank S. Capitani for many useful discussions. We thank R. Sommer for sending us the updated values of β at the matching scale used in this work, and we thank G. Schierholz for sending us, prior to publication, the values of the proton bare matrix element. The computer center at NIC/DESY Zeuthen provided the necessary technical help and the computer resources. This work was supported by the EU IHP Network on Hadron Phenomenology from Lattice QCD and by the DFG Sonderforschungsbereich/Transregio SFB/TR9-03.

Appendix

For the computation of the matrix elements the quark fields are chosen to be periodic in the three space directions,

$$\psi(x + L\hat{k}) = \psi(x), \quad \bar{\psi}(x + L\hat{k}) = \bar{\psi}(x). \quad (47)$$

The lattice derivatives in the forward direction are given by

$$\nabla_\mu \psi(x) = \frac{1}{a} [U(x, \mu) \psi(x + a\hat{\mu}) - \psi(x)] \quad (48)$$

$$\nabla_\mu^* \psi(x) = \frac{1}{a} [\psi(x) - U(x - a\hat{\mu}, \mu)^{-1} \psi(x - a\hat{\mu})] \quad (49)$$

and the backward derivatives are defined by

$$\bar{\psi}(x) \overleftarrow{\nabla}_\mu = \frac{1}{a} [\bar{\psi}(x + a\hat{\mu}) U(x, \mu)^{-1} - \bar{\psi}(x)] \quad (50)$$

$$\bar{\psi}(x)\overleftarrow{\nabla}_\mu^* = \frac{1}{a}[\bar{\psi}(x) - \bar{\psi}(x - a\hat{\mu})U(x - a\hat{\mu}, \mu)]. \quad (51)$$

References

- [1] R. Devenish and A. Cooper-Sarkar, *Deep Inelastic Scattering*, Oxford University Press, Oxford, 2004.
- [2] S. Alekhin, Phys. Rev. **D63** (2001) 094022.
- [3] A.D. Martin, R.G. Roberts, W.J. Stirling, R.S. Thorne, hep-ph/0308087.
- [4] J. Blümlein and H. Böttcher, Nucl. Phys. **B636** (2002) 225.
- [5] R. Petronzio, Nucl. Phys. B (Proc. Suppl.) **73** (1999) 303;
M. Göckeler, R. Horsley, D. Pleiter, P.E.L. Rakow, A. Schäfer and G. Schierholz, Nucl. Phys. B (Proc. Suppl.) **119** (2003) 32;
S. Capitani, Nucl. Phys. B (Proc. Suppl.) **116** (2003) 115;
K. Jansen, to be published in Nuclear Physics A, proceedings of FB17, Durham, USA, 2003;
A. Shindler, to be published in the proceedings of DIS04.
- [6] A. Bucarelli, F. Palombi, R. Petronzio and A. Shindler, Nucl. Phys. **B552** (1999) 379.
- [7] M. Guagnelli, K. Jansen and R. Petronzio, Nucl. Phys. **B542** (1999) 395.
- [8] M. Guagnelli, K. Jansen and R. Petronzio, Phys. Lett. **B457** (1999) 153.
- [9] M. Guagnelli, K. Jansen and R. Petronzio, Phys. Lett. **B459** (1999) 594.
- [10] M. Guagnelli, K. Jansen and R. Petronzio, Phys. Lett. **B493** (2000) 77.
- [11] ZeRo coll.: M. Guagnelli, K. Jansen, F. Palombi, R. Petronzio, A. Shindler and I. Wetzorke, Nucl. Phys. **B664** (2003) 276.
- [12] talk presented by K. Jansen at the XXXth International Conference on High Energy Physics (ICHEP 2000), July 27-August 2, 2000, hep-lat/0010038.
- [13] M. Guagnelli, K. Jansen, F. Palombi, R. Petronzio, A. Shindler and I. Wetzorke, plenary talk given by A. Shindler Electron-Nucleus Scattering VII, June 24-28, 2002, Elba, Eur.Phys.J. **A17** (2003) 365.
- [14] M. Guagnelli, K. Jansen, F. Palombi, R. Petronzio, A. Shindler and I. Wetzorke, World Scientific, Genoa 2002, Gerasimov-Drell-Hearn sum rule and the spin structure of the nucleon, 69-76.
- [15] K. Jansen, Nucl. Phys. B (Proc. Suppl.) **129-130** (2004) 3.
- [16] C. Bernard et. al., Nucl. Phys. B (Proc. Suppl.) **106** (2002) 199.

- [17] M. Lüscher, R. Narayanan, P. Weisz and U. Wolff, Nucl. Phys. **B384** (1992) 168;
S. Sint, Nucl. Phys. **B421** (1994) 135; S. Sint, Nucl. Phys. **B451** (1995) 416;
K. Jansen, C. Liu, M. Lüscher, H. Simma, S. Sint, R. Sommer, P. Weisz and U. Wolff, Phys. Lett. **B372** (1996) 275;
M. Lüscher, S. Sint, R. Sommer and P. Weisz, Nucl. Phys. **B478** (1996) 365.
- [18] R. Sommer, *Lectures at Schladming 1997*, hep-lat/9711243.
- [19] M. Lüscher, *Lectures given at the Les Houches Summer School “Probing the Standard Model of Particle Interactions”, July 28 - September 5, 1997*, hep-lat/9802029.
- [20] R. Sommer, Nucl. Phys. B (Proc. Suppl.) **119** (2003) 185.
- [21] ZeRo coll.: M. Guagnelli, K. Jansen, F. Palombi, R. Petronzio, A. Shindler and I. Wetzorke, hep-lat/0403009.
- [22] JLQCD collaboration, Phys. Rev. **D68** (2003) 054502.
- [23] A. W. Thomas, W. Melnitchouk, F.M. Steffens, Phys. Rev. Lett. **85** (2000) 2892.
- [24] W. Detmold et.al., Phys. Rev. Lett. **87** (2001) 172001.
- [25] D. Arndt and M. J. Savage, Nucl. Phys. **A697** (2002) 429.
- [26] J. W. Chen and M.J. Savage, Nucl. Phys. **A707** (2002) 452.
- [27] S.R. Beane and M.J. Savage, Phys. Rev. **D68** (2003) 114502.
- [28] J. W. Chen, X. Ji Phys. Rev. Lett. **88** (2002) 052003.
- [29] Sutton, Martin, Roberts, Stirling, Phys. Rev. **45** (1992) 2349;
Glück, Reya, Schienbein, Eur.Phys.J.C10 (1999) 313.
- [30] M. Baake, B. Gemünden and R.Oedingen, J. Math. Phys. **23** (1982) 944;
J.E.Mandula, G.Zweig and J.Govaerts, Nucl. Phys. **B228** (1983) 91.
- [31] ALPHA coll.:M. Guagnelli *et al.*, Nucl. Phys. **B560** (1999) 465.
- [32] ALPHA coll.:M. Lüscher *et al.*, Nucl. Phys. **B491** (1997) 323.
- [33] B. Sheikholeslami and R. Wohlert, Nucl. Phys. **B259** (1985) 572.
- [34] S.Capitani *et al.*, Nucl. Phys. B (Proc. Suppl.) **63** (1998) 153;
S.Capitani *et al.*, Nucl. Phys. **B544** (1999) 669.
- [35] R. Sommer, *private communication*.

- [36] S. Necco and R. Sommer, Nucl. Phys. **B622** (2002) 328.
- [37] O.V. Tarasov, A.A. Vladimirov, A.Yu. Zharkov, Phys. Lett. **B93** (1980) 429.
- [38] E.G. Floratos, D.A. Ross, C.T. Sachrajda, Nucl. Phys. **B129** (1977) 66;
Erratum: Nucl. Phys. **B139** (1978) 545;
A. Gonzalez-Arroyo, C. Lopez, F.J. Yndurain, Nucl. Phys. **B153** (1979) 161;
G. Curci, W. Furmanski, R. Petronzio, Nucl. Phys. **B175** (1980) 27.
- [39] R. Sommer, Nucl. Phys. **B411** (1994) 839; M. Guagnelli, R. Sommer, H. Wittig
Nucl. Phys. **B535** (1998) 389.
- [40] C. Best *et al.*, Phys. Rev. **56** (1997) 2743.
- [41] ZeRo Coll.: A. Shindler, M. Guagnelli, K. Jansen, F. Palombi, R. Petronzio
and I. Wetzorke, Nucl. Phys. B (Proc. Suppl.) **129-130** (2004) 278.
- [42] G. Schierholz, *private communication*.
- [43] LHPC coll.: D. Dolgov *et al.*, Phys. Rev. **D66** (2002) 034506.

$\beta = 6/g_0^2$	κ	c_{sw}	Fit interval	m_π	Fit interval	$\langle x \rangle$
6.0	0.153	0	14 - 21	0.4205(14)	12 - 20	0.3080(18)
	0.154	0	14 - 20	0.3606(17)	12 - 20	0.2994(24)
	0.155	0	14 - 19	0.2924(21)	13 - 19	0.2876(38)
6.1	0.151605	0	17 - 31	0.3685(05)	17 - 25	0.3073(12)
	0.152500	0	17 - 30	0.3120(06)	17 - 25	0.2951(16)
	0.153313	0	16 - 29	0.2536(07)	16 - 26	0.2799(21)
6.2	0.150600	0	19 - 35	0.3147(09)	20 - 28	0.3037(21)
	0.151300	0	19 - 34	0.2674(10)	20 - 28	0.2918(27)
	0.151963	0	18 - 33	0.2163(12)	20 - 28	0.2763(38)
6.3	0.149259	0	22 - 46	0.2968(08)	22 - 42	0.3033(20)
	0.149978	0	22 - 45	0.2481(10)	21 - 43	0.2888(29)
	0.150604	0	21 - 44	0.1996(12)	19 - 45	0.2704(44)
6.45	0.1486	0	29 - 51	0.2045(06)	28 - 44	0.2854(23)
	0.1489	0	29 - 50	0.1808(07)	28 - 44	0.2767(27)
	0.1492	0	30 - 49	0.1547(08)	28 - 44	0.2652(35)
6.0	0.1334	NP [32]	15 - 20	0.4021(13)	14 - 18	0.2704(21)
	0.1338	NP	14 - 20	0.3551(13)	14 - 18	0.2667(26)
	0.1342	NP	14 - 19	0.3028(16)	15 - 17	0.2636(41)
6.1	0.1340	NP	17 - 46	0.3534(05)	16 - 40	0.2671(14)
	0.1345	NP	17 - 46	0.2947(05)	16 - 40	0.2579(17)
	0.1350	NP	17 - 43	0.2239(06)	16 - 40	0.2467(26)
6.2	0.1346	NP	19 - 33	0.2798(07)	19 - 29	0.2624(18)
	0.1349	NP	18 - 32	0.2430(08)	19 - 29	0.2567(23)
	0.1352	NP	18 - 32	0.2008(09)	18 - 30	0.2500(29)
6.3	0.1346	NP	21 - 42	0.2640(07)	22 - 42	0.2643(16)
	0.1349	NP	21 - 42	0.2284(07)	22 - 42	0.2573(20)
	0.1352	NP	21 - 42	0.1881(08)	21 - 43	0.2467(26)
6.45	0.1348	NP	26 - 52	0.2040(05)	26 - 46	0.2566(19)
	0.1350	NP	25 - 51	0.1791(05)	26 - 45	0.2502(24)
	0.1352	NP	25 - 50	0.1513(06)	27 - 45	0.2426(31)

Table 2: Results for the pseudoscalar mass and the bare matrix element at all our simulation points. We specify also the fit interval for the effective mass and the bare matrix element obtained from the request of having the systematic uncertainty coming from the excited states below 0.1% and 0.4%, respectively. See text for further details.

L/a	$\beta = 6/g_0^2$	κ_c	c_{sw}	$Z_{\mathcal{O}_{44}}^{SF}$	$Z_{\mathcal{O}_{12}}^{SF}$
8	6.0055	0.153597(14)	0	0.3211(44)	0.3673(35)
10	6.1425	0.152277(10)	0	0.2994(43)	0.3467(35)
12	6.2670	0.151024(7)	0	0.3008(43)	0.3462(33)
16	6.4825	0.149012(12)	0	0.2861(57)	0.3262(44)
8	6.0055	0.135006(5)	NP [32]	0.3451(37)	0.3423(31)
10	6.1425	0.135625(4)	NP	0.3204(36)	0.3260(31)
12	6.2670	0.135756(3)	NP	0.3131(35)	0.3287(30)
16	6.4825	0.135617(4)	NP	0.3029(43)	0.3167(37)

Table 3: Results for $Z_{\mathcal{O}_{44}}^{SF}$ and $Z_{\mathcal{O}_{12}}^{SF}$ at the scale $\mu_0 = (1.436r_0)^{-1}$ with Wilson and non-perturbatively improved clover actions.

c_{sw}	applicability	i	z_i^{SF}	z_i^{RGI}
0	$6.0 \leq \beta \leq 6.5$	0	0.3197	1.446
		1	-0.1166	-0.527
		2	0.1046	0.473
NP [32]	$6.0 \leq \beta \leq 6.5$	0	0.3451	1.561
		1	-0.1806	-0.817
		2	0.1962	0.888

Table 4: Coefficients of the interpolating polynomials, eq. (36) and (42). Uncertainties are discussed in the text.

$m_\pi^2 [\text{GeV}^2]$	$\langle x \rangle^{\overline{\text{MS}}} (\mu = 2 \text{ GeV})$
1.000	0.312(20)
0.900	0.306(17)
0.800	0.300(15)
0.700	0.293(14)
0.600	0.285(13)
0.500	0.279(13)
0.400	0.274(14)
0.315	0.269(15)
0.000	0.246(15)

Table 5: Results for the matrix element in the continuum limit (quenched approximation), converted to the $\overline{\text{MS}}$ scheme at 2 GeV. The continuum extrapolation was performed with a constrained linear fit of the Wilson and non-perturbatively improved clover data for the four smaller lattice spacings. The value in the chiral limit is obtained from a linear fit (see text for details).